Electronic Supplementary Material (ESI) for Inorganic Chemistry Frontiers.


# A new 0D-2D $CsPbBr_3$-$Co_3O_4$ heterostructure photocatalyst with efficient charge separation for photocatalytic $CO_2$ reduction

Xin Zhong,[a†] Xinmeng Liang,[a†] Xinyu Lin,[a] Jin Wang,*[a,b] Malik Zeeshan Shahid,*[a] and Zhengquan Li,*[a,b]

[a]Key Laboratory of the Ministry of Education for Advanced Catalysis Materials, Zhejiang Normal University, Jinhua, Zhejiang 321004, P. R. China.

[b]Zhejiang Institute of Optoelectronics, Zhejiang Normal University, Jinhua, Zhejiang 321004, P. R. China.

[#] The authors contributed equally.

**Corresponding Author**

* E-mail: wangjin@zjnu.edu.cn

* E-mail: zeeshan-nano@zjnu.edu.cn

* E-mail: zqli@zjnu.edu.cn

# TABLE OF CONTENTS

# 1. EXPERIMENTAL SECTION

## 1.1 Materials

All chemicals were purchased and used without further purification. Lead bromide $PbBr_2$ (99.999%), $Cs_2CO_3$ (99.995%), oleic acid (OA, $C_{18}H_{34}O_2$, 90%), and octadecene (ODE, $C_{18}H_{36}$, 99.8%), were purchased from Sigma-Aldrich. Hexane (95%), cyclohexamethylenetetramine (Urotropine, 99.5%, $C_6H_{12}N_4$), ethanol, and ethyl acetate (EA, 99.8%) were purchased from Aladdin company. Chloride hexahydrate (99%, $CoCl_2.6H_2O$) was purchased from Sinopharm chemical reagent. The water used for the experiments was purified by a Millipore Milli-Q system.

## 1.2 Characterization

Transmission electron microscopy (TEM), high-resolution TEM (HRTEM), high-angle annular dark-field scanning transmission electron microscopy (HAADF-STEM), and energy-dispersive X-ray spectroscopy (EDS) were measured by employing a JEOL JEM-2100F field-emission high-resolution transmission electron microscope operated at 200 kV. The samples were prepared by using EA solution, and a piece of the carbon-coated copper grid was used on which a drop of suspension (of each sample) was precisely placed. The copper grid was dried under ambient conditions and further used for morphological characterization. Zeta sizer Nano-ZS (Malvern Instruments, U.K.) was used to collect Zeta (ζ)-potential data, for which the samples were prepared by dispersing in EA solutions. Philips X'Pert Pro Super X-ray diffractometer with Cu-Kα radiation (λ =1.5418Å) was used to record Powder XRD patterns. Shimadzu 2501PC UV-vis spectrophotometer was employed to investigate the UV-vis absorption spectra. FluoroMax-4 spectrofluorometer (HoribaScientific) and analyzed with an Origin-integrated software (FluoroEssencev2.2) was used to measure the steady-state photoluminescence (PL) spectra. The PL decay spectra were recorded on a photoluminescence spectrometer (FLS980, Edinburgh Instruments Ltd.) with a 380-nm excitation wavelength and a 515-nm emission wavelength with the time-correlated single-photon counting (TCSPC) mode. The lifetime data were analyzed with DataStation v6.6 (Horiba Scientific). ESCALab 250 X-ray photoelectron spectrometer with Al-Kα radiation was used to record X-ray photoelectron spectra (XPS) data in which the calibration was done with C 1s peak at 284.6 eV.

## 1.3 Photocatalytic activity measurement

In a typical experiment, the as-prepared photocatalysts (5 mg) were first added to a Pyrex photoreactor without using any sacrificial agent. Next, 50 µL of water was added. Then, a rubber septum was used to seal the photoreactor, and then it was vacuumed and subsequently purged with $CO_2$ for 10~20 min in the dark. The photoreactor was then placed in a water bath maintained at 25 °C, stirred, and irradiated by a 300-W Xe lamp with a 400 nm cutoff filter (Solaredge 700, 100 $mW \cdot cm^{-2}$). The product distribution was quantified through periodic headspace gas analysis (500 µL) by gas chromatography (GC, 7820A, Ar carrier, Agilent). Produced $CH_4$ was measured by a flame ionization detector (FID), and CO was converted to $CH_4$ by a methanation reactor and then analyzed by the FID. The isotope-labelled experiments were performed using $^{13}CO_2$ instead of $^{12}CO_2$, and the products were analyzed using gas chromatography-mass spectrometry (GC-MS, 7890A and 5975C, Agilent). The products were separated with GC in advance and reached the MS at different retention times.

## 1.4 Photoelectrochemical measurements

The Photoelectrochemical measurements were carried out using a three-electrode cell CHI 760E electrochemical station (Shanghai Chenhua, China) with a Pt foil counter electrode and a saturated Ag/AgCl reference electrode. The working electrode was prepared by the dip-coating method. About 1 mg of the photocatalyst was dispersed in 1 mL of hexane and 10 µL Nafion solution to form a slurry. Next, 30 µL of the slurry was dip-coated on the FTO conductive glass with an exposure area of 0.196 $cm^2$. Subsequently, the film was dried in a vacuum oven at 80 $^oC$. Then acetonitrile solution with 0.1 mol/L of tetrabutylammonium hexafluorophosphate ($TBAPF_6$) was used as the electrolyte. The variation of photoinduced current density versus time (I-t curve) was recorded at a 0 V bias potential under visible light switching on and off mode, $\lambda > 400$ nm, 300 W Xe lamp (Solaredge 700). The electrochemical impedance spectroscopy (EIS) results were obtained at the open circuit potential using a frequency ranging from $10^4$ Hz to $10^{-1}$ Hz.

## 1.5 Energy bandgap calculations

In relational expression proposed by Tauc, Devis, and Mott i.e., $\alpha h\nu = A (h\nu - E_g)^n$ symbols are denoted as follows; h: plank constant, v: frequency of vibration, α: absorption coefficient, $E_g$: band gap, and A: proportional constant. As both constituents i.e., $CsPbBr_3$ QDs and $Co_3O_4$ HPs

in heterostructure are direct allowed transition, the calculation of energy bandgap value was based on n=1/2.

# 2. SUPPLEMENTARY FIGURES S1-13

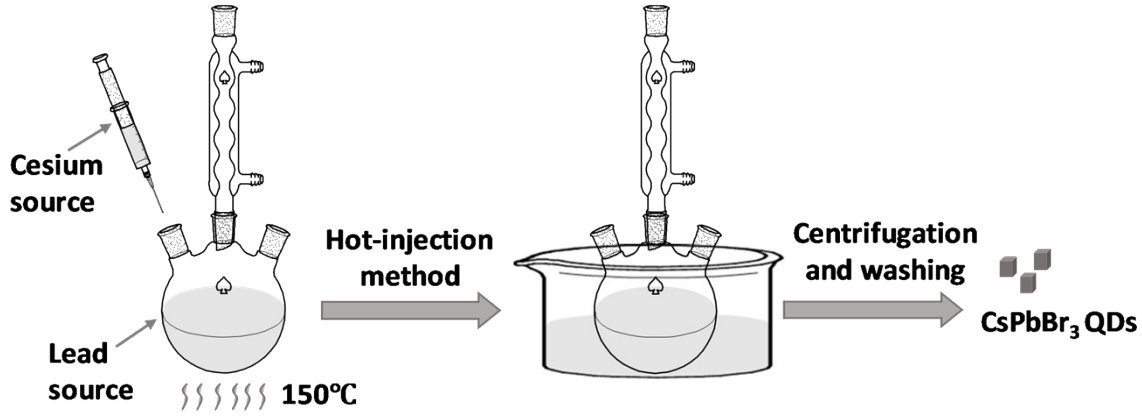


**Fig. S1** Schematic illustration for the synthesis of $CsPbBr_3$ QDs via hot-injection method.

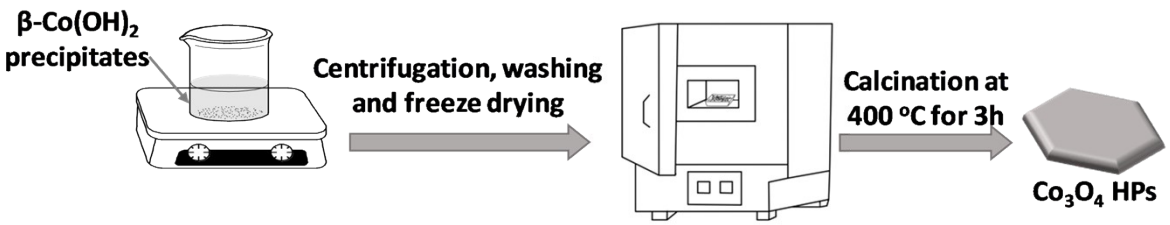


**Fig. S2** Schematic illustration for the synthesis of $Co_3O_4$ HPs by calcination route.

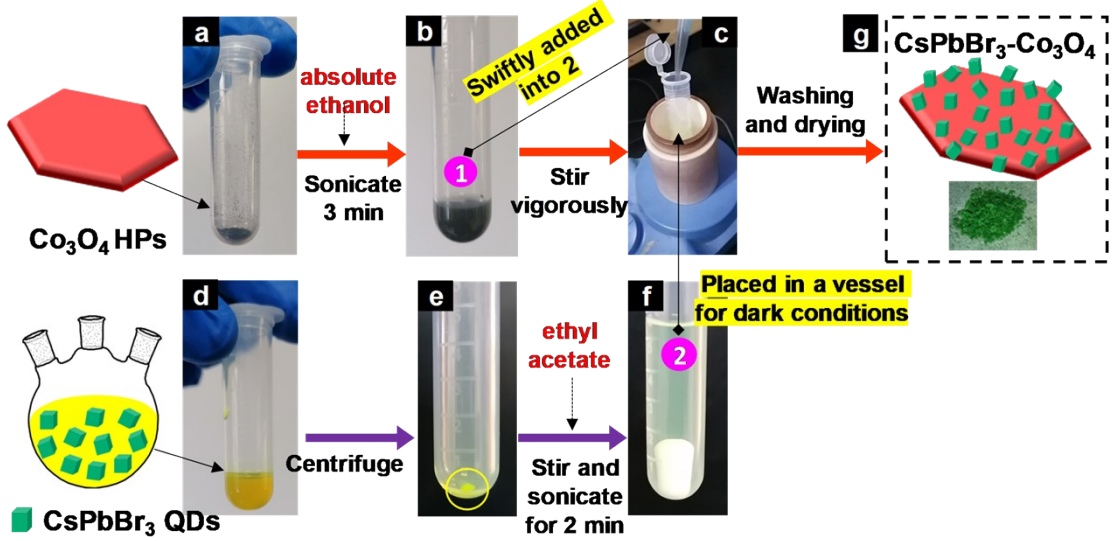


**Fig. S3** Illustration for the synthesis 0D/2D $CsPbBr_3$-$Co_3O_4$ heterostructure at ambient conditions, indicating stepwise processes and their real-time photographs.

The desired quantity of $Co_3O_4$ HPs was taken (Fig. S3a) and dissolved in absolute ethanol via sonication for 3 minutes (Fig. S3b) to get suspension 1. On the other hand, the required amount of $CsPbBr_3$ QDs was taken from stock (Fig. S3d), centrifuged (Fig. S3e), and dispersed in ethyl acetate via stirring and sonication for 2 minutes to obtain the suspension 2 (Fig. S3f). This suspension 2 was then placed in the Teflon linen vessel for the subsequent procedure to occur in the dark (Fig. 1c). Next, suspension 1 was swiftly inserted into suspension 2 under vigorous stirring (Fig. 1c), and later on, covered with another Teflon linen vessel directed upside down to achieve a dark environment. The stirring continued for 30 minutes in dark and another 30 minutes in ambient conditions and finally, after washing and drying, the $CsPbBr_3$-$Co_3O_4$ heterostructure was obtained(Fig. S3g).

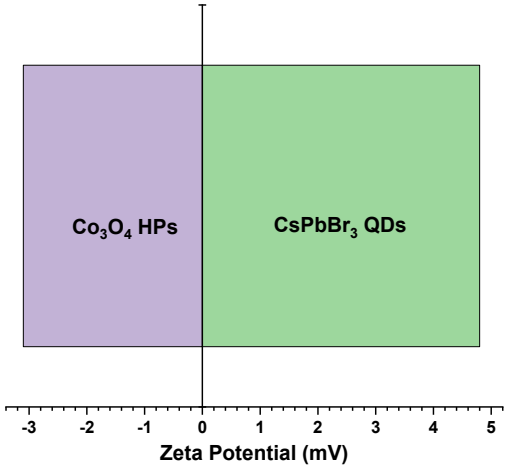


**Fig. S4** Zeta potential of pristine $Co_3O_4$ HPs and $CsPbBr_3$ QDs in the solution of ethyl acetate. The values endorsing the successful coulomb electrostatic interaction between these components to form the $Co_3O_4$-$CsPbBr_3$ heterojunction.

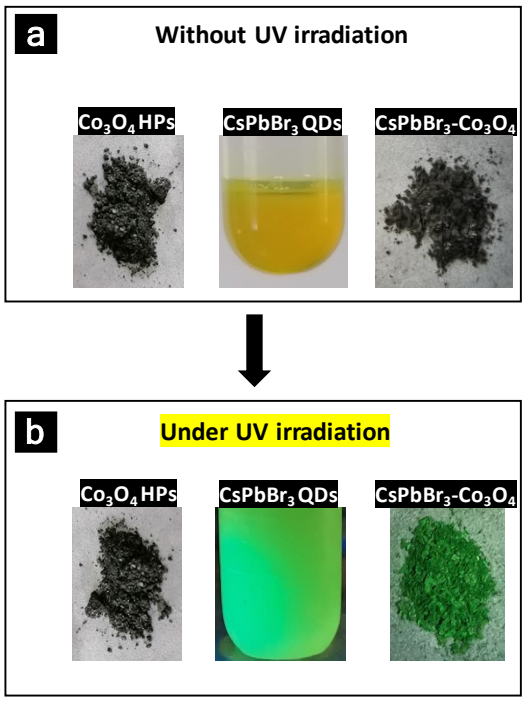


**Fig. S5** Color transformations of as-prepared samples (a) without UV light irradiation and (b) under UV light illumination.

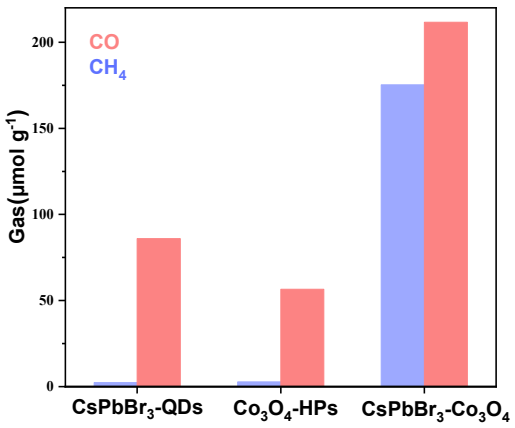


**Fig. S6** Comparative depiction of catalytic activity during 6 hours in terms of produced gas CO and $CH_4$ by using as-synthesized $CsPbBr_3$ QDs, $Co_3O_4$ HPs, and $CsPbBr_3$-$Co_3O_4$ heterostructure.

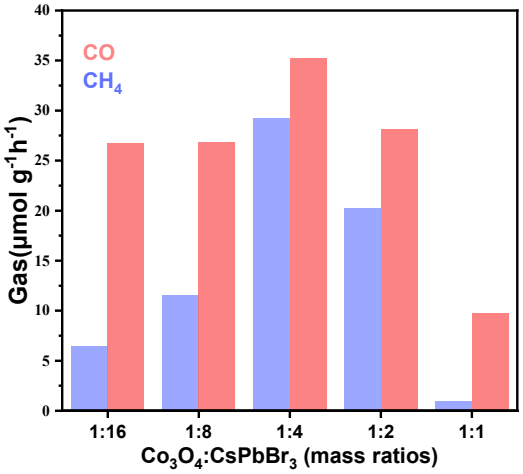


**Fig. S7** Influence of various mass ratios in the $CsPbBr_3$-$Co_3O_4$ heterostructure over the production of CO and $CH_4$.

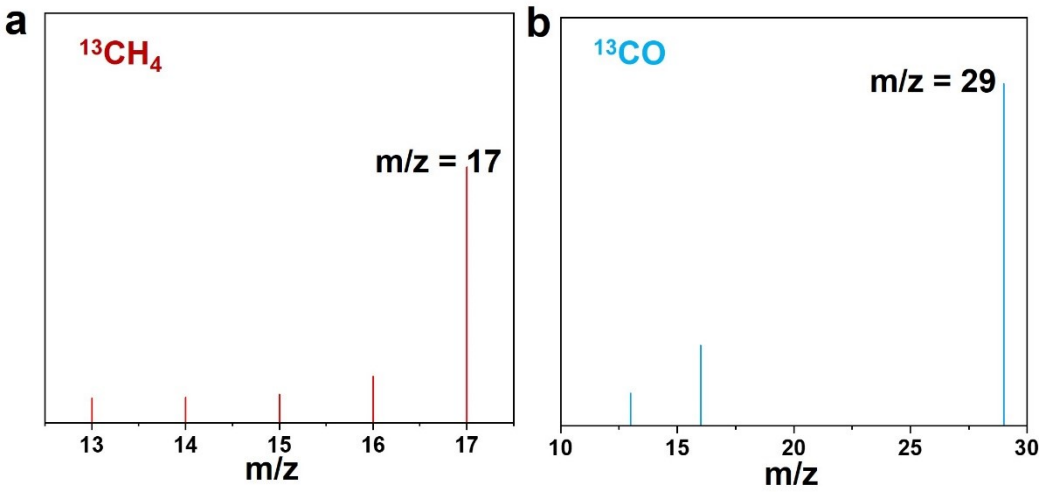


**Fig. S8** Mass spectra showing (a) $^{13}CH_4$ (m/z = 17) and (b)$^{13}CO$ (m/z = 29) generated over $CsPbBr_3$-$Co_3O_4$ in the photocatalytic $^{13}CO_2$ reduction.

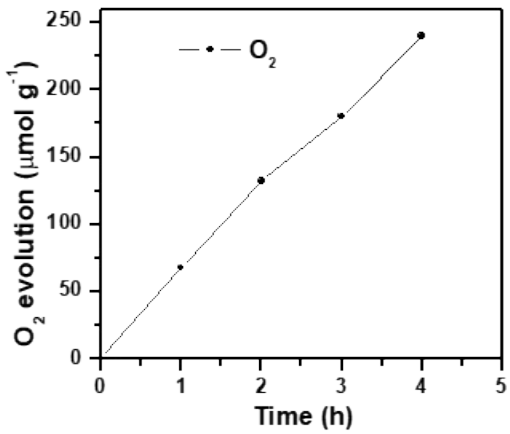


**Fig. S9** The results confirm the oxidation of water to oxygen during the photocatalytic reduction of $CO_2$.

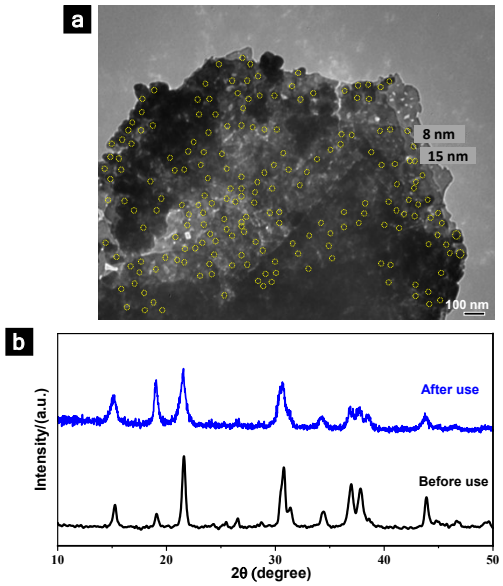


**Fig. S10** TEM image and XRD pattern of $CsPbBr_3$-$Co_3O_4$ after 5 consecutive cycles, displaying the stability of both morphology and crystallinity, beneficial for practical applications.

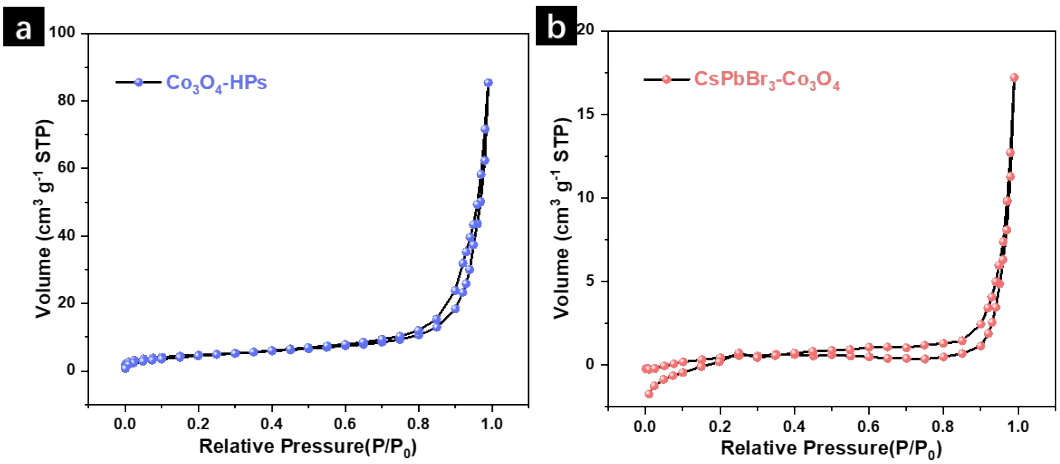


**Fig. S11** Nitrogen adsorption-desorption curves for (e) pristine $Co_3O_4$ HPs and (f) $Co_3O_4$ HPs decorated with $CsPbBr_3$-QDs, and their corresponding Brunauer-Emmett-Teller BET surface area values are mentioned in Table S1.

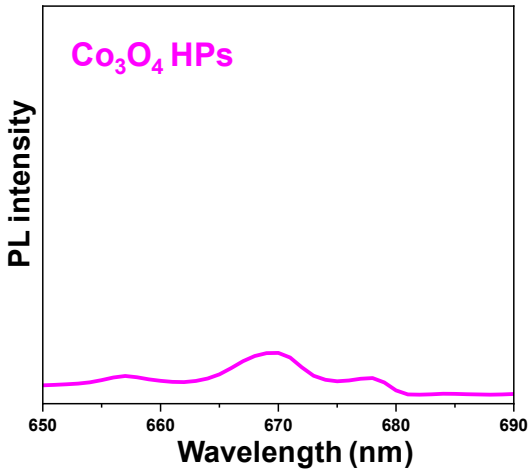


**Fig. S12** Control experiments showing steady-state photoluminescence spectra of $Co_3O_4$ HPs.

Under an excitation wavelength at about 630 nm, a weak PL signal was obtained. The peak at 670 nm was probably ascribed to deep-level emission in $Co_3O_4$. Note that the as-prepared $Co_3O_4$ sample did not display the signals for TRPL.

# 3. SUPPLEMENTARY TABLES S1-3

**Table S1.** The photocatalytic activity of various state-of-the-art photocatalysts in comparison with as-prepared $CsPbBr_3$-$Co_3O_4$ heterostructure

| Entry# | Photocatalyst | CO | $CH_4$ | *$R_{electron}$ | Reference |
|---|---|---|---|---|---|
| | | μmol $g^{-1}h^{-1}$ | | | |
| 1 | $CsPbBr_3$-$Co_3O_4$ | 35.40 | 29.2 | 304.4 | This work |
| 2 | $CsPbBr_3$ QDs | 14.23 | 0.39 | 31.98 | This work |
| 4 | $CsPbBr_3$-BiOBr | 2.5 | 26.1 | 213.8 | [1] |
| 5 | $BiVO_4$/$CsPbBr_3$ | 17 | 6 | 82 | [2] |
| 6 | Mn-$CsPbBr_3$ | 7.5 | 0.58 | 19.64 | [3] |
| 7 | ZnSe−$CsSnCl_3$ | 57 | 2 | 128.32 | [4] |
| 8 | $CsPbBr_3$/CTF-1 | 48.2 | 0 | 96.4 | [5] |
| 9 | 0D $CsPbBr_3$/2D $CsPb_2Br_5$ | 197.11 | 1.5 | 406.22 | [6] |
| 10 | $CsPbBr_3$/$Bi_2WO_6$ | 50.3 | 1 | 108.6 | [7] |
| 11 | $CsPbBr_3$/$Bi_2WO_6$ | 9.3 | 14.3 | 133 | [8] |
| 12 | $CsPbBr_3$/UiO-66($NH_2$) | 8.21 | 0.26 | 18.5 | [9] |
| 13 | $CsPbBr_3$ QDs | 4.125 | 1.90 | 23.72 | [10] |
| 14 | $CsPbBr_3$ /GO | 4.81 | 2.46 | 29.32 | [10] |
| 15 | $Co_3O_4$ (OVs) | 51.7 | 0 | 103.4 | [11] |
| 16 | $Co_3O_4$/$Al_2O_3$ | 48.4 | 0 | 96.8 | [12] |
| 17 | Hollow $Co_3O_4$ Dodecahedron | 46.3 | 0 | 92.6 | [13] |
| 18 | $Co_3O_4$ nanoparticles | 0.73 | 10 | 81.48 | [14] |

*Formula used to calculate the rate of electron consumed: $R_{electron} = 2R_{CO} + 8R_{CH_4}$

Where $R_{CO}$ is the rate of CO evolution, and $R_{CH_4}$ is the rate of $CH_4$ evolution

**Table S2.** The information of nitrogen adsorption-desorption analysis in terms of BET surface area, average pore size, and total pore volume of as-synthesized $Co_3O_4$-HPs and $CsPbBr_3$-$Co_3O_4$.

| **Samples** | **BET surface area** | **average pore size** | **total pore volume** |
|---|---|---|---|
| | **($m^2/g$)** | **(nm)** | **($cm^3/g$)** |
| $Co_3O_4$ HPs | 16.902 | 31.35 | 0.1325 |
| $CsPbBr_3$-$Co_3O_4$ | 5.016 | 21.21 | 0.0266 |

**Table S3.** PL decay parameters of the $CsPbBr_3$ QDs in comparison with $CsPbBr_3$-$Co_3O_4$ heterostructure.

| **Sample** | $\tau_1$ | $A_1$ | $\tau_2$ | $A_2$ | $\tau_3$ | $A_3$ | $\tau_{avg}$ |
|---|---|---|---|---|---|---|---|
| $CsPbBr_3$-QDs | 2.61 | 72.9% | 14.71 | 23.7% | 104.36 | 3.4% | 47.43 |
| $CsPbBr_3$-$Co_3O_4$ | 3.38 | 7.5% | 18.21 | 84.2% | 103.52 | 8.3% | 45.04 |
| *Determined using the fitting function $y = B + A_1 \exp(-t/\tau_1) + A_2 \exp(-t/\tau_2) + A_3 \exp(-t/\tau_3)$ | | | | | | | |

# 4. REFERENCES


1 Z. Zhang, L. Li, Y. Jiang and J. Xu, Step-scheme photocatalyst of $CsPbBr_3$ quantum Dots/BiOBr nanosheets for efficient $CO_2$ photoreduction, *Inorg.chem.*, 2022, **61**, 3351-3360.

2 X. Y. Yue, L. Cheng, J. J. Fan and Q. J. Xiang, 2D/2D $BiVO_4$/$CsPbBr_3$ S-scheme heterojunction for photocatalytic $CO_2$ reduction: Insights into structure regulation and Fermi level modulation, *Appl. Catal. Environ.*, 2022, **304**, 120979.

3 C. C. Lin, T. R. Liu, S. R. Lin, K. M. Boopathi, C. H. Chiang, W. Y. Tzeng, W. C. Chien, H. S. Hsu, C. W. Luo, H. Y. Tsai, H. A. Chen, P. C. Kuo, J. Shiue, J. W. Chiou, W. F. Pong, C. C. Chen and C. W. Chen, Spin-polarized photocatalytic $CO_2$ reduction of Mn-doped perovskite nanoplates, *J. Am. Chem. Soc.*, 2022, **144**, 15718-15726.

4 N. Li, X. Chen, J. Wang, X. Liang, L. Ma, X. Jing, D. L. Chen and Z. Li, ZnSe Nanorods-$CsSnCl_3$ perovskite heterojunction composite for photocatalytic $CO_2$ reduction, *ACS nano*, 2022, **16**, 3332-3340.

5 Q. Wang, J. Wang, J. C. Wang, X. Hu, Y. Bai, X. Zhong and Z. Li, Coupling $CsPbBr_3$ quantum dots with covalent triazine frameworks for visible-light-driven $CO_2$ reduction, *ChemSusChem*, 2021, **14**, 1131-1139.

6 L. Ding, B. Borjigin, Y. Li, X. Yang, X. Wang and H. Li, Assembling an affinal 0D $CsPbBr_3$/2D $CsPb_2Br_5$ architecture by synchronously in situ growing $CsPbBr_3$ QDs and $CsPb_2Br_5$ nanosheets: enhanced activity and reusability for photocatalytic $CO_2$ reduction, *ACS applied mater. interfaces*, 2021, **13**, 51161-51173.

7 J. Wang, J. Wang, N. Li, X. Du, J. Ma, C. He and Z. Li, Direct Z-scheme 0D/2D heterojunction of $CsPbBr_3$ quantum Dots/$Bi_2WO_6$ nanosheets for efficient photocatalytic $CO_2$ reduction, *ACS Appl. Mater. Interfaces*, 2020, **12**, 31477-31485.

8 Y. Jiang, H. Y. Chen, J. Y. Li, J. F. Liao, H. H. Zhang, X. D. Wang and D. B. Kuang, Z-Scheme 2D/2D heterojunction of $CsPbBr_3$/$Bi_2WO_6$ for improved photocatalytic $CO_2$ reduction, *Adv. Func. Mater.*, 2020, **30**, 2004293.

9 S. Wan, M. Ou, Q. Zhong and X. Wang, Perovskite-type $CsPbBr_3$ quantum dots/UiO-66($NH_2$) nano junction as efficient visible-light-driven photocatalyst for $CO_2$ reduction, *Chem. Eng. J.*, 2019, **358**, 1287-1295.

10 Y. F. Xu, M. Z. Yang, B. X. Chen, X. D. Wang, H. Y. Chen, D. B. Kuang and C. Y. Su, A $CsPbBr_3$ perovskite quantum dot/graphene oxide composite for photocatalytic $CO_2$ reduction, *J. Am. Chem. Soc.*, 2017, **139**, 5660-5663.

11 Q. Zhang, P. Yang, H. Zhang, J. Zhao, H. Shi, Y. Huang and H. Yang, Oxygen vacancies in $Co_3O_4$ promote $CO_2$ photoreduction, *Appl. Catal. Environ.*, 2022, **300**, 120729.

12 P. Yang, Q. Zhang, Z. Yi, J. Wang and H. Yang, Rational electronic control of carbon dioxide reduction over cobalt oxide, *J. Catalysis*, 2020, **387**, 119-128.

13 L. Wang, J. Wan, Y. Zhao, N. Yang and D. Wang, Hollow multi-shelled structures of $Co_3O_4$ dodecahedron with unique crystal orientation for enhanced photocatalytic $CO_2$ reduction, *J. Am. Chem. Soc.*, 2019, **141**, 2238-2241.

14 J. Y. Choi, C. K. Lim, B. Park, M. Kim, A. Jamal and H. Song, Surface activation of cobalt oxide nanoparticles for photocatalytic carbon dioxide reduction to methane, *J. Mater. Chem.*, 2019, **7**, 15068-15072.